Synthesis and chiral resolution of a triply twisted Möbius carbon nanobelt

Wei Fan,[1,+] Toshiya M. Fukunaga,[2,+] Shaofei Wu,[1] Yi Han,[1] Qifeng Zhou,[1,3] Jinyi Wang,[1] Zhengtao Li,[1] Xudong Hou,[1] Haipeng Wei,[1] Yong Ni,[1] Hiroyuki Isobe,[2,*] Jishan Wu[1,3,*]

[1]Department of Chemistry, National University of Singapore, 3 Science Drive 3, 117543, Singapore

[2]Department of Chemistry, The University of Tokyo, Hongo, Bunkyo-ku, Tokyo 113-0033, Japan

[3]Joint School of National University of Singapore and Tianjin University, International Campus of Tianjin University, Bin-hai New City, Fuzhou 350207, China

[+]These authors contributed equally to this work

* Correspondence to: isobe@chem.s.u-tokyo.ac.jp (HI), chmwuj@nus.edu.sg (JW)

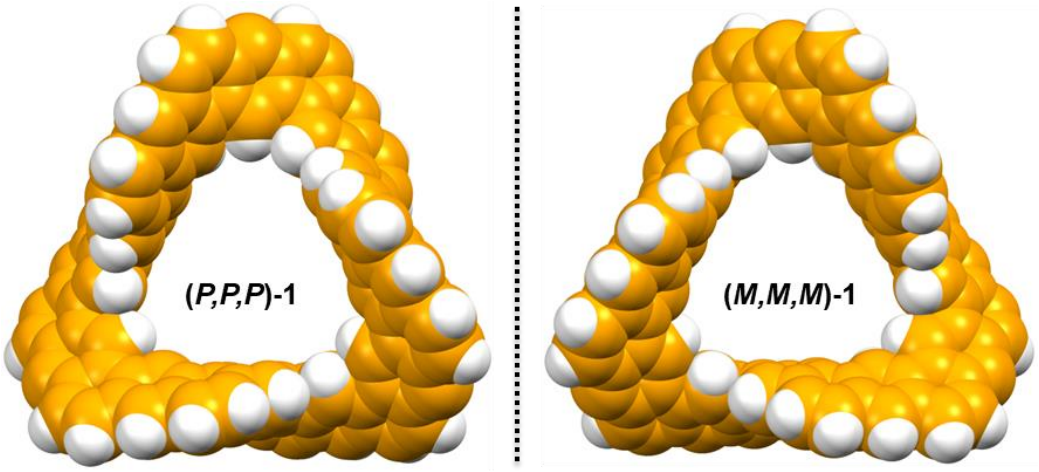

Abstract:

Atomically precise synthesis of topological molecular carbons such as Möbius carbon nanobelts (MCNBs) represents a big challenge in synthetic organic chemistry as it requires careful control of both twist and strain. So far, only one singly twisted MCNB has been reported and the MCNBs with more than two twists remain unknown. Herein, we report the facile synthesis of the first triply twisted MCNB by rational design and via a synthetic route involving Suzuki coupling-mediated macrocyclization, $Bi(OTf)_3$-catalyzed cyclization of vinyl ethers, followed by oxidative dehydrogenation. The Möbius band-like structure was unambiguously confirmed by X-ray crystallographic analysis, which also revealed coexistence of (*P*,*P*,*P*)- and (*M*,*M*,*M*)- enantiomers. The racemic isomers were resolved by chiral HPLC and the isolated enantiomers exhibited a large absorption dissymmetry factor ($|g_{abs}|$ = 0.019) according to circular dichroism spectroscopy, which can be explained by the fully conjugated structure and the desirable orientation of the electric and magnetic transition moments.

Main text:

Topological molecular carbons such as twisted and knotted carbon nanostructures are attracting increasing attention not only because they are aesthetically beautiful, but also due to their promising applications for electronics, photonics and spintronics.[1-3] Among them, Möbius strip-like molecules with an odd number of twists are of particularly interest (Fig. 1a)[4] because they are topologically chiral, and they can serve as model compounds to validate the theoretically predicted [4*n*] Möbius aromaticity.[5] Synthesis of this type of molecules is extremely challenging as one needs to carefully control both structural flexibility and large strain induced by the twist. The first non-conjugated Möbius molecule was synthesized by Walba *et al* in 1982 via a macro-etherification reaction,[6] while the first π-conjugated all-hydrocarbon Möbius molecule was reported by Herges and co-workers in 2003,[7] which also demonstrated weak Möbius aromaticity. Later on, Latos-Grażyński and Osuka's teams independently discovered Möbius aromaticity and antiaromaticity in expanded porphyrinoids.[8-12]

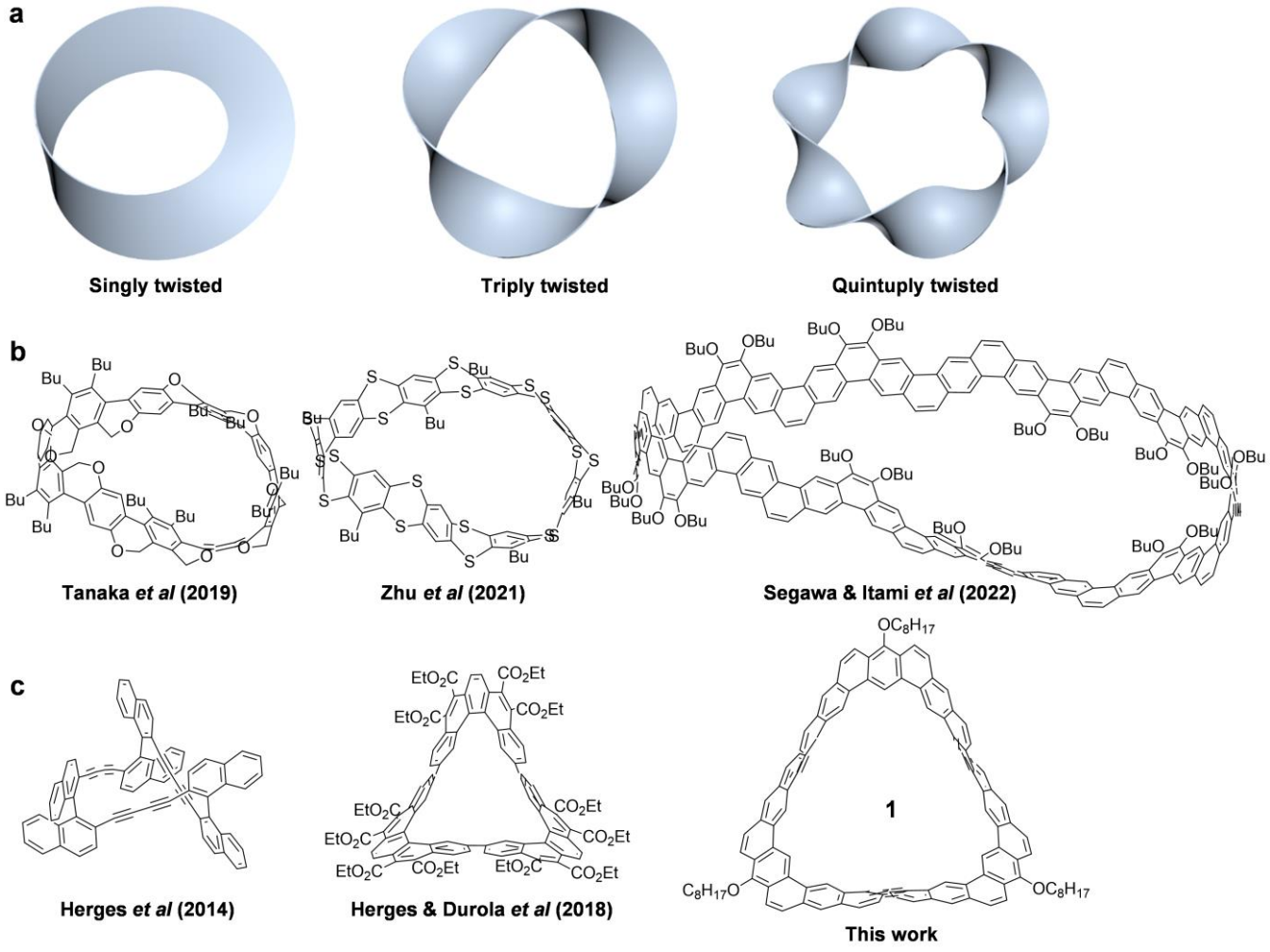

Fig 1. Möbius strip-like molecules with an odd number of twists. **a.** Schematic representation of singly, triply and quintuply twisted Möbius molecules. **b**. Reported double-stranded Möbius belts with single twist. **c**. Reported single-stranded Möbius molecules with three twists, and the new triply twisted carbon nanobelt (**1**) in this work.

The last decade has witnessed a rapid growth of a family of topological molecular carbons, the cyclo-*para*-phenylenes (CPPs), which are also called as "carbon nanohoops".[13] The synthetic methods developed by Jast,[14] Itami,[15] Yamago[16] and Isobe[17] *et al* nicely solved the long-standing problem arisen from the large strain in the final CCP rings. Inspired by these

progresses, chemists are now moving on to synthesize even more challenging carbon nanostructures such as twisted and knotted molecules containing fully conjugated units. For example, a number of CPP-based Möbius strip-like[18-20] or mechanically interlocked molecules[21-22] have been reported. These structures mainly contain single-stranded CPP rings and thus the π-conjugation is limited due to the significant tortional angles between the 1,4-phenylene units. Therefore, double-stranded, fully π-conjugated Möbius nanobelts become new targets. In 2019, Tanaka and coworkers reported the efficient synthesis of a CPP-based Möbius belt with a single twist and double strands by employing rhodium-catalyzed alkyne cyclotrimerization (Fig. 1b).[23] Later, in 2021, Zhu and co-workers reported a sulfur-embedded, double-stranded Möbius-shaped belt (Fig. 1b) mainly by using Ullmann-type couplings followed by intramolecular Friedel-Crafts reactions.[24] However, these two double-stranded Möbius molecules are not fully conjugated because their backbones are linked partially by either saturated (–CH_2O–) or sulfur atom (–S–) linkers. Finally, in 2022, Itami, Segawa, and their co-workers reported the synthesis of the first singly twisted, double-stranded, all-sp^2 Möbius carbon nanobelt (MCNB) over 14 steps via Z-selective Wittig reactions followed by nickel-mediated intramolecular homocoupling reactions (Fig. 1b).[25] The successfully isolated (25,25)MCNB was calculated to have a strain energy of about 49.4 kcal/mol, while the attempted synthesis of smaller-size MCNBs failed due to their larger strain. Different from the singly twisted Möbius structures, the Möbius systems with higher twists (e.g., the triply and quintuply twisted) (Fig. 1a) could have smaller strain energy per each twist and thus synthetically it may be more accessible from the viewpoint of strain energy. On the other hand, it requires more careful control on the conformation at each twist due to the structural flexibility.[26, 27] So far, only two π-conjugated, triply twisted Möbius molecules have been reported by Herges, Durola, and their co-workers (Fig. 1c).[28,29] Again, due to their single-stranded structure, the cyclic π-conjugation is limited. Therefore, a highly twisted MCNB with a fully conjugated double-stranded structure remains exclusive. Herein, we report the facile synthesis of the first triply twisted MCNB (**1**, Fig. 1c) by rational design, and its chiral resolution which gave two enantiomers showing promising chiroptical properties.

Results and discussion

Design and synthesis

The key for the synthesis of a triply twisted MCNB relies on the control of both twist and strain, and a suitable reaction to form double-stranded fully conjugated structure. We recently demonstrated that $Bi(OTf)_3$-mediated cyclization of vinyl ethers[30] was an efficient benzannulation reaction for the synthesis of double-stranded kekulene, cycloarenes, and expanded kekulenes.[31-32] This reaction was also successfully applied for the synthesis a twisted carbon nanobelt with a figure-eight geometry.[33] In that case, pre-organization of each constitutional aromatic unit and vinyl ether group in the semi-rigid precursor allows regio-selective cyclization to form a rigid, double-stranded carbon nanobelt with two half twists. Encouraged by these successful examples, we designed a synthetic strategy for a triply twisted MCNB (**1**, Fig. 2) based on the following considerations: (i) To control the conformation at each twist, two key building blocks, a C_2 symmetric 5,6,12,13-tetrahydrobenzo[*k*]tetraphene (THBT) with two Bpin groups at 2,9-positions (**4**) and a 1,3-dibromobenzene carrying two vinyl ether groups at 2,4-positions (**5**), were chosen. Such design would allow the formation of a semi-rigid macrocycle (**3a** or **3b**) with three-fold symmetry after Suzuki coupling reactions. Due to the steric hindrance between the vinyl ether groups and the nearby THBT units, the dihydronaphthalene

moieties in **4** that linked to the benzene ring in **3** could adopt an alternating "up" and "down" orientation relative to the mean plane of the macrocycle to partially release the strain. In fact, DFT calculations also predict that this triply twisted structure has lower energy (about 5.3 kcal/mol) than the other conformer (Fig. S16 in Supplementary Information). Such a pre-organization would lead to regio-selective cyclization of vinyl ethers to the specific carbon sites on the THBT units (highlighted in Fig. 2) at the next step to give a more rigid, double-stranded macrocycle (**2a** or **2b**). (ii) To avoid possible problems arisen from the large strain during the benzannulation step, two sp^3-hybridized ethylene units rather than sp^2- carbon-carbon double bonds are introduced in the building block **4**. This would result in less strain in the nanobelt **2a**/**2b** as compared to the fully conjugated MCNB **1**. Conversion of **2a**/**2b** to **1** could be done by aromaticity-driven oxidative dehydrogenation reaction at the last step. (iii) To balance solubility and crystallinity, *n*-butoxy (**5a**) or *n*-octyloxy (**5b**) is introduced onto the building block. The former substituent allows us to obtain single crystals of the key intermediate **2a**, while the latter endows sufficient solubility of the final MCNB **1** for isolation as well as growth of single crystals.

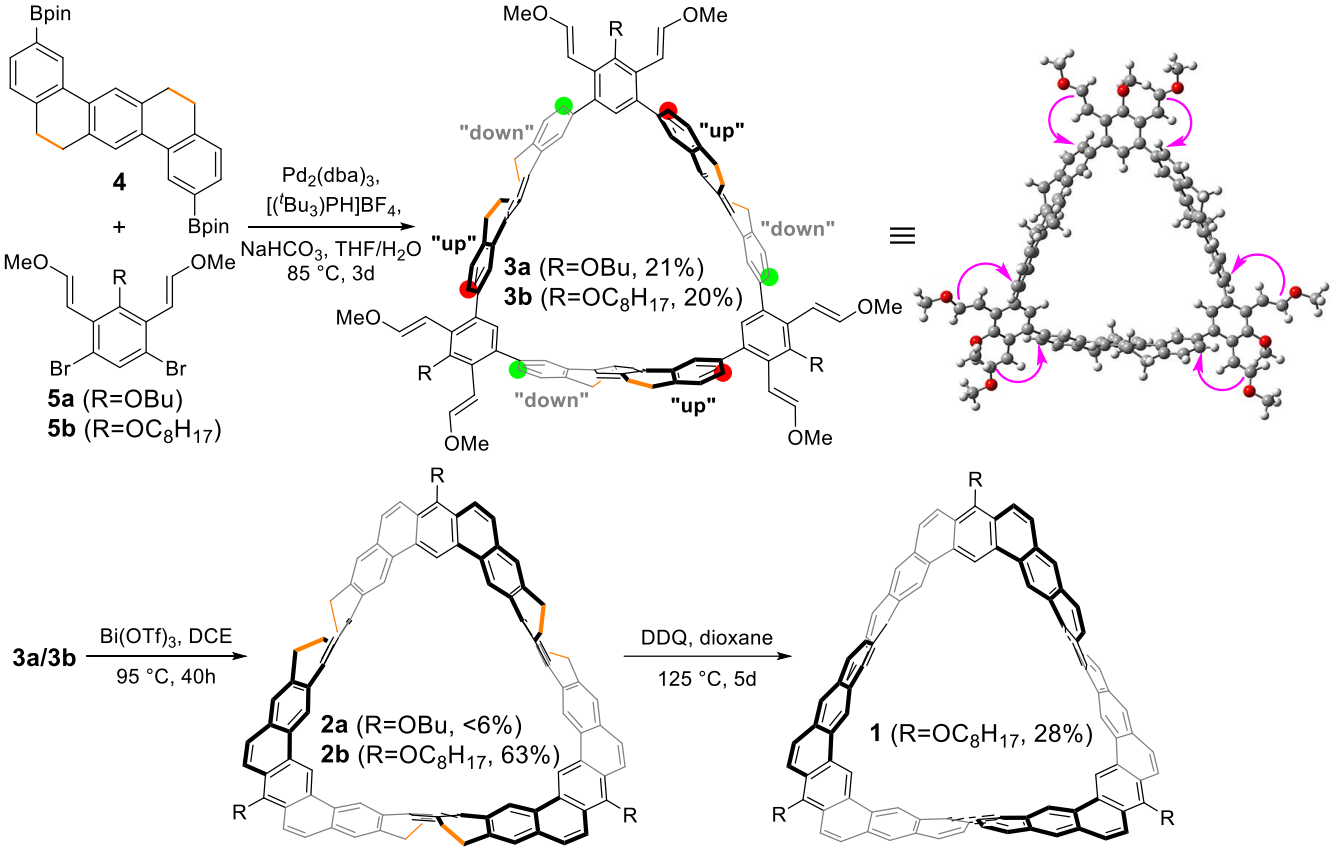

Fig 2. **Synthetic route of the triply twisted Möbius carbon nanobelt 1**. The red and green dots in **3a**/**3b** highlight the cyclization sites on the benzene rings that bent outward ("up") and inward ("down") the paper plane, respectively. The optimized geometry of **3a**/**3b** (in which the alkoxy groups are replaced by methoxy during the calculation) is also shown, with the pink arrows indicating the regio-selective electrophilic cyclization.

The key building block **4** was isolated as a "side-product" of its *cis*-isomer in our previous report.[33] Compounds **5a** and **5b** were synthesized starting from 3,5-dibromo-2,6-dimethylphenol[34] via multiple steps involving alkylation, bromination, hydrolysis, oxidation, and Wittig reaction (Scheme S1 in Supplementary Information). The Suzuki coupling reactions between **4** and **5a**/**5b** in dilute solutions gave macrocycles **3a**/**3b** in 21%/20% yield after purification by preparative GPC. The ^{1}H NMR spectra of **3a**/**3b** recorded in CD_2Cl_2 indicated a

highly symmetrical structure at room temperature (Fig. S51, S53 in Supplementary Information). Subsequent $Bi(OTf)_3$-mediated cyclization reaction of **3b** afforded the double-stranded nanobelt **2b** in 63% yield. However, the same reaction on **3a** yielded a poorly soluble nanobelt **2a**, leading to less than 6% isolated yield. Nevertheless, single crystals of **2a** suitable for X-ray crystallographic analysis were successfully obtained at this stage, which clearly confirmed by triply twisted Möbius band structure (see below). Finally, oxidative dehydrogenation of **2b** by 2,3-dichloro-5,6-dicyano-1,4-benzoquinone (DDQ) in dioxane at 125 ^oC after 5 days gave the fully π-conjugated MCNB **1** in 28% isolated yield. Compound **1** has moderate solubility in THF and is stable under the ambient conditions. Its structure was unambiguously confirmed by X-ray crystallographic analysis, NMR, and high-resolution mass spectrometry (see Supplementary Information). The racemic isomers of **2b** and **1** were successfully resolved by chiral HPLC, which allowed us to investigate their chiroptical properties.

X-ray crystallographic structures

Single crystals of **3a** were grown by slow diffusion of methanol into its solution in carbon disulfide/toluene with a volume ratio of 1:1. X-ray crystallographic analysis revealed a triply twisted Möbius geometry containing six saturated CH_2−CH_2 bonds (Fig. 3a). The existence of saturated single bonds in **3a** effectively releases the strain during the cyclization reaction. Both (*P,P,P*)- and (*M,M,M*)-enantiomers have been observed in the crystal structure in equal amount, and they are arranged in an alternating mode in each layer, forming a tight two-dimensional polymer network with close π−π contacts (distances of 2.8−2.9 Å) (Fig. 3b and Fig. S30 in Supplementary Information). Between the adjacent layers, there exist multiple [CH···π] and van der Waals interactions (distances of 2.7−2.9 Å) (Fig. 3b), which result in a densely packed three-dimensional (3D) structure (Fig. 3c). As for **1**, although it has three long alkoxy substituents (-OC_8H_{17}), the fully conjugated and highly symmetric structure allows itself for high crystallinity. The single crystals of **1** were obtained from slow diffusion of methanol into its solution in 1,1,2,2-tetrachloroethane. X-ray crystallographic analysis disclosed a fully conjugated, all sp^2-hybridized, triply twisted Möbius topological structure (Fig. 3d). However, the (*P,P,P*)- and (*M,M,M*)-enantiomers of **1** are not equally found in the crystal structure but with a ratio of 1:2 (Fig. 3e and Fig. S30 in Supplementary Information). Some close π−π contacts (distances of 2.7−3.4 Å) are observed between two enantiomers for each layer and multiple [CH···π] and van der Waals interactions (distances of 2.7−2.9 Å) also exist between the adjacent layers (Fig. 3e). The sum of these short contact interactions and the existence of long alkoxy chains renders a relatively loose 3D structure of **1** in the single crystal as compared to **3a** (Fig. 3f). Bond length analysis of **3a** and **1** indicated a dominant double bond nature for the newly fused -CH=CH- moieties like kekulene and other cycloarenes[31-33] (Fig. S29 in Supplementary Information), indicating a localized aromatic character in these nanobelts (see further discussion below).

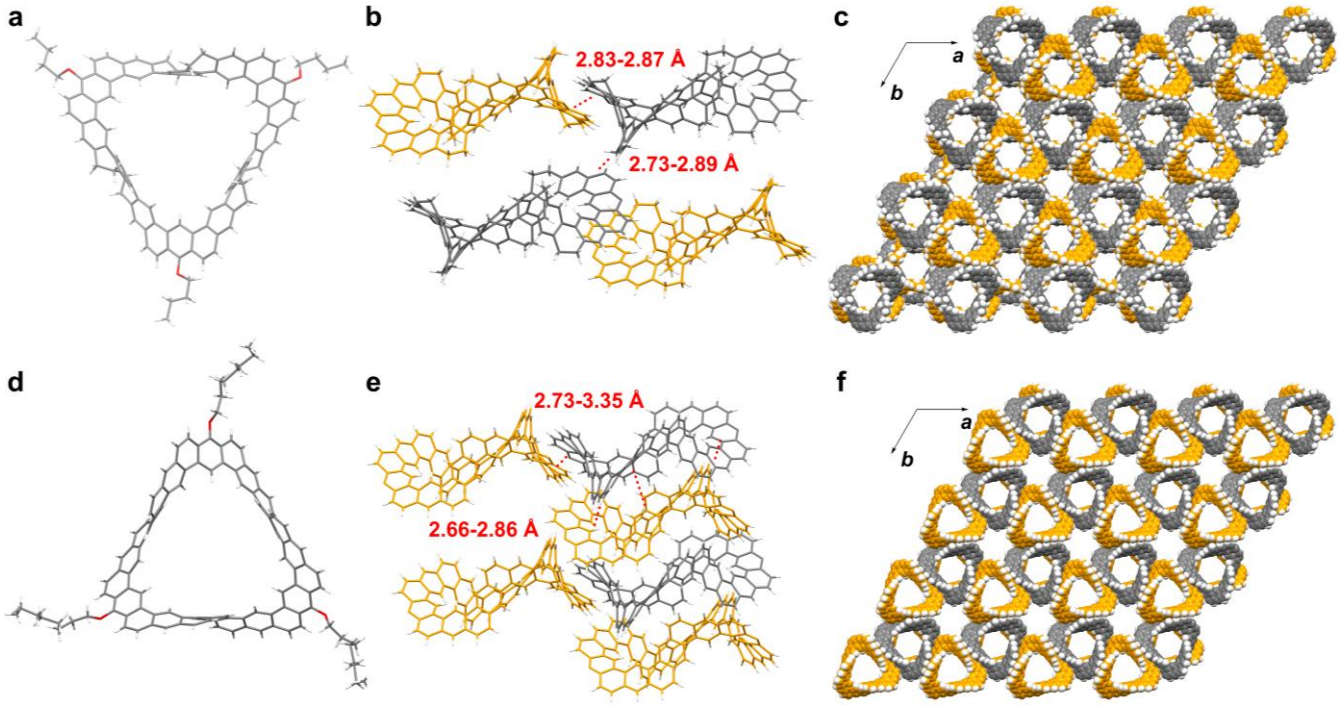

Fig 3. X-ray crystallographic structures. (**a**-**c**) for **2a** and (**d**-**f**) for **1**. The backbone structures with grey and yellow color represent (*P,P,P*)-enantiomers and (*M,M,M*)-enantiomers, respectively. The red and white color atoms represent O and H, respectively. The ORTEP drawing has 50% thermal probabilities. Some of the substituents were removed for clarity.

Strain energy analysis

Theoretical calculations (B3LYP-6-31G(d,p)) based on hypothetical homodesmotic reactions predict that the total strain is about 68.2 kcal/mol for the precursor **2a**/**2b**, while around 103.9 kcal/mol for the fully conjugated MCNB **1** (Fig. S17 in Supplementary Information). The much smaller strain energy in **2a**/**2b** as compared to **1** indicates that the introduction of the THBT unit containing saturated -CH_2-CH_2- moieties is crucial for the successful cyclization reaction. The increased strain energy in the last oxidative dehydrogenative step can be partially compensated by the gained aromatic stabilization energy. In addition, the average strain energy for each twist in the triply twisted MCNB **1** is around 34.6 kcal/mol, which is smaller than that in the singly twisted (25,25)MCNB (49.4 kcal/mol).[25] Moreover, the strain could be visualized along the molecular backbone through StrainViz developed by Jasti and co-workers.[35] As shown in Fig. 4a-b and Fig. S18, the total strain energy of **2a**/**2b** is calculated as 110.8 kcal/mol, while the maximum strain energy of an individual bond is 1.9 kcal/mol. The corresponding strain energies of **1** also increase to 142.3 kcal/mol and 2.4 kcal/mol, respectively (Fig. 4c-d). Most of the strains for both **2a**/**2b** and **1** are vastly located on the twist positions along the inner rims (Fig. 4).

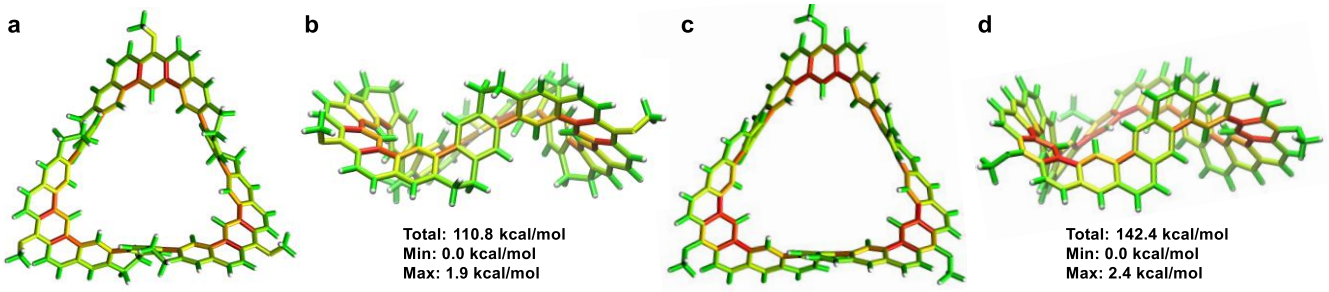

Fig 4. **Calculated StrainViz maps**. **a.** Top view and **b.** side view for **2a**/**2b**. **c.** Top view and **d.** side view for **1**. The bonds bearing high, medium and low strain are shown in red, yellow and green, respectively. The substituent groups are replaced by methoxy groups during the calculations.

Electronic structure and aromaticity

The ^{1}H NMR spectra (aromatic region) of **2a**, **2b**, and **1** in 1,1,2,2-tetrachloroethane-d_2 are shown in Fig. S1 and 2D ROESY technique was used for the detailed assignment (Fig. S5-S11 in Supplementary Information). The chemical shifts for **2a** and **2b** are almost the same, indicating that the protons of both molecules are in a similar chemical environment. The ^{1}H NMR spectrum of **1** has two additional doublet peaks in the aromatic region, which originate from the dehydrogenated saturated bonds (-CH_2-CH_2-). The peak for the central benzene ring in each THBT unit in **2a**/**2b** (δ = 7.1 ppm) was shifted to a lower field in **1** (δ = 8.2 ppm), resulting from a fully π-conjugated skeleton with a dominant local aromatic character. The variable-temperature (VT) NMR spectra for these three compounds did not exhibit obvious change with temperature elevation (Fig. S2-S4 in Supplementary Information) due to their rigid and twisted skeletons. Nuclear-independent chemical shift (Fig. S23 in Supplementary Information) and anisotropy of the induced current density (Fig. S24-S25 in Supplementary Information) calculations on **2a**/**2b** and **1** suggest a dominant localized aromatic character, in accordance with the bond length analysis. 3D isochemical shielding surface (ICSS) calculations reveal that the shielding regions (depicted in blue) are mainly located on the backbone of **2a**/**2b** and **1** (Fig. 5a-b and Fig. S26-S27). The deshielding regions (depicted in red) for **2a**/**2b** are along with the shielding region but interrupted at the saturated bonds. On the other hand, the deshielding region of **1** intertwines the shielding region and forms an interesting trefoil strip (Fig. 5b), which is similar to the boundary of a triply twisted trefoil knot. To further understand the electronic structure of **1**, the localized orbital locator isosurface of π orbitals (LOL-π)[36-38] calculation was also performed. The map of LOL-π reveals that **1** has just one phase of π orbitals which are delocalized along the whole skeleton (shown in red, Fig. 5c), confirming a fully conjugated structure with single π-surface.

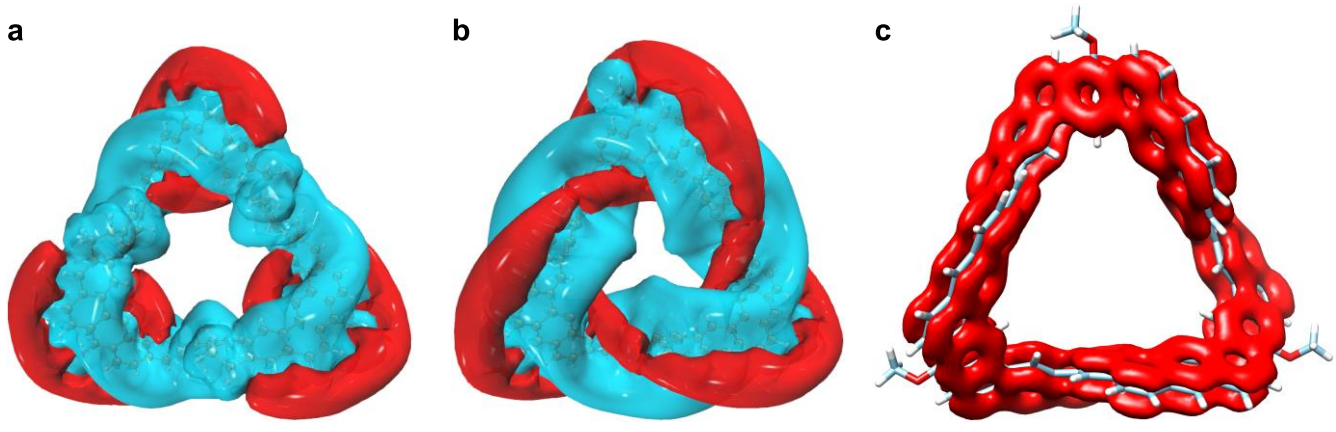

Fig 5. **Calculated 3D ICSS maps and LOL-π isosurface**. **a**. 3D ICSS map for **2a**/**2b**. **b**. 3D ICSS maps for **1** (blue, isovalue = 1; red, isovalue = -0.5). **c**. Calculated LOL-π isosurface of **1** (isovalue = 0.2). The substituent groups are replaced by methoxy groups during the calculations.

Photophysical and chiroptical properties

Compound **2b** in dichloromethane (DCM) shows well-resolved absorption spectrum with five major vibronic peaks at 336, 351, 373, 392, and 424 nm (Fig. 6a). Compound **1** displays a

more intense absorption spectrum with the major absorption peaks at 382, 413 and 470 nm, which are red-shifted as compared to **2b**, in accordance with the extended π-conjugation pathway. However, due to the localized aromatic character, the shift is not significant. The absorption band with peak at 470 nm can be correlated to partially allowed HOMO→LUMO electronic transition (oscillator strength f = 0.0014) according to the time-dependent (TD) DFT calculations (Table S2 in Supplementary Information). The HOMO and LUMO coefficients are delocalized along the whole backbone (Fig. 6b), again indicating a fully conjugated electronic structure. Compound **2b** and **1** exhibit similar well-resolved fluorescence spectra with two major emission peaks at 462/486 nm and 486/518 nm, respectively (Fig. 6a). The slightly red-shifted emission band in **1** as compared to **2b** can be explained by the same reasons. The absolute fluorescence quantum yields (FLQY) of **2a** and **1** in DCM was determined to be 62.0% and 13.6%, respectively, by using integrating sphere technique. The relatively low FLQY of **1** could be ascribed to its small oscillator strength for the $S_0 \rightarrow S_1$ transition, which however will benefit absorption dissymmetry factor of their enantiomers.[39] Furthermore, their corresponding fluorescence lifetimes were measured as 7.3 ns and 6.7 ns, respectively.

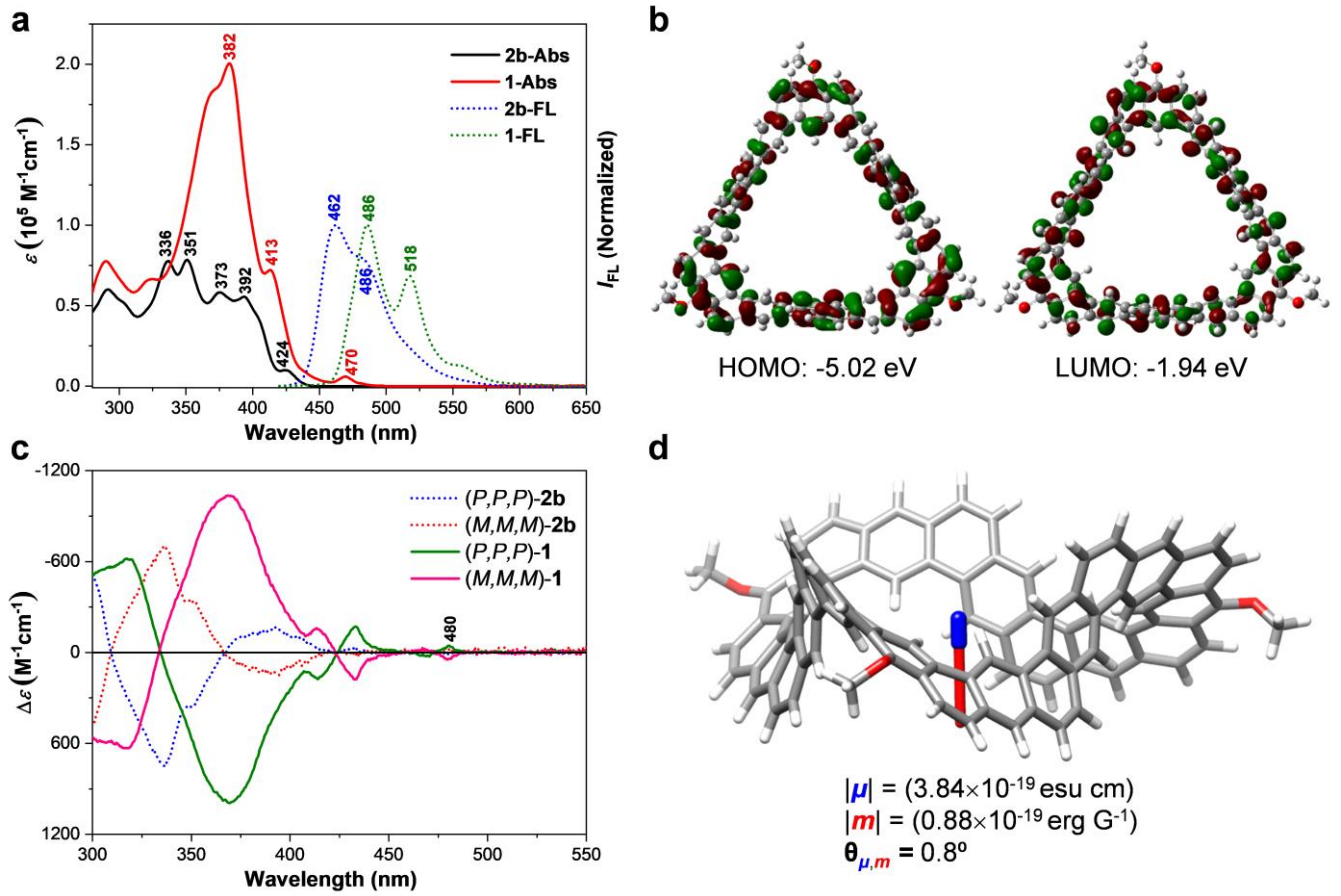

Fig 6. **Photophysical and chiroptical properties. a**. UV−vis absorption (Abs) and normalized fluorescence (FL) spectra of **2b** and **1** measured in DCM. **b**. Calculated HOMO and LUMO profiles and energies. **c**. CD spectra of (*P,P,P*)-**2b**, (*M,M,M*)-**2b**, (*P,P,P*)-**1**, and (*M,M.M*)-**1** recorded in DCM. **d**. Calculated transition dipole moments for the $S_0 \rightarrow S_1$ electronic transitions in (*M,M,M*)**- 1**. The electric transition dipole moments (***μ***) are shown in blue, and the magnetic transition dipole moments (***m***) are shown in red.

The chiral resolution of **2b** and **1** were successfully achieved by using chiral HPLC (Fig. S12 in Supplementary Information). The absolute configurations were assigned as $(+)_{380}$-**2b** = (*P,P,P*)-**2b**/$(-)_{380}$-**2b** = (*M,M,M*)-**2b**, while $(+)_{380}$-**1** = (*P,P,P*)-**1**/$(-)_{380}$-**1** = (*M,M,M*)-**1** based on

experimental (Fig. 6c) and theoretical (Fig. S13 in Supplementary Information) circular dichroism (CD) spectra. The largest absorption dissymmetry factor $|g_{abs}|$ value of 0.012 for **2b** is recorded from higher energy transitions, and there is also a very small $|g_{abs}|$ value (< 0.001) through S_0-S_1 transition. In contrast, **1** has the largest $|g_{abs}|$ value of 0.019 originating from the S_0-S_1 transition. The larger g_{abs} value of **1** may be owing to its D_3 symmetric, fully conjugated, triply twisted Möbius structure while possess an ideal topology for electric transitions to enhance magnetic transition dipole moment.[40] According to the calculations of dissymmetry factor, g value can be simplified as the equation: $g = 4|\boldsymbol{\mu}||\boldsymbol{m}|\cos\theta/(|\boldsymbol{\mu}|^2 + |\boldsymbol{m}|^2)$, wherein $\boldsymbol{\mu}$, $\boldsymbol{m}$, and θ are the electric transition dipole moment, the magnetic transition dipole moment, and the angle between $\boldsymbol{\mu}$ and $\boldsymbol{m}$, respectively.[39] For most single organic molecules, $|\boldsymbol{m}| \ll |\boldsymbol{\mu}|$, thus, the key point to improve the g value is to suppress $\boldsymbol{\mu}$ and extend $\boldsymbol{m}$, meanwhile keeping the angle between $\boldsymbol{\mu}$ and $\boldsymbol{m}$ to approach 0º or 180º. In our cases, the $|g_{abs}|$ value around 424 nm for **2b** is originated from $S_0 \rightarrow S_1$, $S_0 \rightarrow S_2$ and $S_0 \rightarrow S_3$ transitions according to the TD DFT calculations (Table S1 in Supplementary Information), while $S_0 \rightarrow S_2$ and $S_0 \rightarrow S_3$ transitions with large oscillator strength (f = 0.95) made the major contributions. The calculated $|g_{abs}|$ value of **2b** for $S_0 \rightarrow S_2/S_3$ transitions with large $|\boldsymbol{\mu}|$ and small $|\boldsymbol{m}|$ value, and not perfect angle θ (76.8º) between them is 0.001 (Fig. S23 and Table S3 in Supplementary Information). The asymmetric electric structures of **2b** caused the very small $|g_{abs}|$ value in the lowest energy level transitions. In contrast, the calculated $|g_{abs}|$ value of **1** for $S_0 \rightarrow S_1$ transition around 480 nm is 0.87 with a smaller $|\boldsymbol{\mu}|$ and larger $|\boldsymbol{m}|$, and a perfect angle θ (0.8º) between them (Fig. 6d and Table S3 in Supplementary Information). The highly symmetric and fully conjugated structure of **1** enables electric transition dipole moment to cancel out in the plane of molecule and form a larger magnetic transition dipole moment, further prompting the two vectors of $|\boldsymbol{\mu}|$ and $|\boldsymbol{m}|$ perpendicular to the molecular plane.

Conclusion

In summary, an all sp^2-hybridized, triply twisted Möbius carbon nanobelt (**1**) with a double-stranded structure was synthesized and isolated in single-crystal form. The success relies on: (i) proper choice of the precursors with saturated -CH_2−CH_2- bonds and preferable bond angles, (ii) efficient macrocyclization by Suzuki coupling reaction to form a triply twisted, pre-organized intermediate with a minimal strain, (iii) regio-selective $Bi(OTf)_3$-catalyzed cyclization reaction of vinyl ethers for benzannulation, and (iv) aromaticity-driven oxidative dehydrogenation at last step to generate the final fully conjugated MCNB with large strain. Based on the experimental and theoretical calculations, **1** has a dominant localized aromatic character. The chiral resolution of **2b** and **1** were successfully achieved, where **1** demonstrated a large absorption dissymmetry factor ($|g_{abs}|$ = 0.019) for the $S_0 \rightarrow S_1$ transition due to its D_3 symmetry, efficient π-conjugation along the skeleton, and favorable alignment of the electric and magnetic transition moments. The synthetic strategy developed in this work could promote the synthesis of diverse topological molecular carbons with persistent chirality in the future.

References

1 Fernández-García, J. M., Evans, P. J., Filippone, S., Herranz, M. Á. & Martín, N. Chiral molecular carbon nanostructures. *Acc. Chem. Res*. **52**, 1565–1574 (2019).

2 Segawa, Y., Levine, D. R. & Itami, K. Topologically unique molecular nanocarbons. *Acc. Chem. Res*. **52**, 2760–2767 (2019).

3 Guo, Q.-H., Jiao, Y., Feng, Y. & Stoddart, J. F. The rise and promise of molecular nanotopology. *CCS Chem*. **3**, 1542–1572 (2021).

4 Rzepa, H. S. Möbius Aromaticity and Delocalization. *Chem. Rev*. **105**, 3697–3715 (2005).

5 Heilbronner, E. Hückel molecular orbitals of Möbius-type conformations of annulenes. *Tetrahedron Lett.* **5**, 1923–1928 (1964).

6 Walba, D. M., Richards, R. M. & Haltiwanger, R. C. Total synthesis of the first molecular Moebius strip. *J. Am. Chem. Soc.* **104**, 3219–3221 (1982).

7 Ajami, D., Oeckler, O., Simon, A. & Herges, R. Synthesis of a Möbius aromatic hydrocarbon. *Nature* **426**, 819–821 (2003).

8 Stępień, M., Latos-Grażyński, L., Sprutta, N., Chwalisz, P. & Szterenberg, L. Expanded porphyrin with a split personality: A Hückel-Möbius aromaticity switch. *Angew. Chem., Int. Ed*. **46**, 7869–7873 (2007).

9 Tanaka, Y. et al. Metalation of expanded porphyrins: a chemical trigger used to produce molecular twisting and Möbius aromaticity. *Angew. Chem., Int. Ed*. **120**, 693–696 (2018).

10 Park, J. K. et al. Möbius aromaticity in N-fused [24]pentaphyrin upon Rh(I) metalation. *J. Am. Chem. Soc*. **130**, 1824–1825 (2008).

11 Pacholska-Dudziak, E. et al. Palladium vacataporphyrin reveals conformational rearrangements involving Hückel and Möbius macrocyclic topologies. *J. Am. Chem. Soc*. **130**, 6182–6195 (2008).

12 Yoon, Z. S., Osuka, A. & Kim, D. Möbius aromaticity and antiaromaticity in expanded porphyrins. *Nat. Chem.* **1**, 113–122 (2009).

13 Lewis, S. E. Cycloparaphenylenes and related nanohoops. *Chem. Soc. Rev.* **44**, 2221-2304 (2015).

14 Jasti, R., Bhattacharjee, J., Neaton, J. B. & Bertozzi, C. R. Synthesis, characterization, and theory of [9]-, [12]-, and [18]cycloparaphenylene: carbon nanohoop structures. J*. Am. Chem. Soc.* **130**, 17646–17647 (2008).

15 Takaba, H., Omachi, H., Yamamoto, Y., Bouffard, J. & Itami, K. Selective synthesis of [12]cycloparaphenylene. *Angew. Chem. Int. Ed.* **48**, 6112–6116 (2009).

16 Yamago, S., Watanabe, Y. & Iwamoto, T. Synthesis of [8]cycloparaphenylene from a square-shaped tetranuclear platinum complex. *Angew. Chem. Int. Ed.* **49**, 757–759 (2010).

17 Hitosugi, S., Nakanishi, W., Yamasaki, T. & Isobe, H. Bottom-up synthesis of finite models of helical (*n*, *m*)-single-wall carbon nanotubes. *Nat. Commun*. **2**, 492 (2011).

18 Qiu, Z. et al. Isolation of a carbon nanohoop with Möbius topology. *Sci. China. Chem.* **64**, 1004–1008 (2021).

19 Malinčík, J. et al. Circularly polarized luminescence in a Möbius helicene carbon nanohoop. *Angew. Chem., Int. Ed*. **61**, e202208591 (2022).

20 Terabayashi, T. et al. Synthesis of twisted [N]cycloparaphenylene by alkene insertion. *Angew. Chem., Int. Ed.* **61**, e202214960 (2022).

21 Segawa, Y. et al. Topological molecular nanocarbons: All-benzene catenane and trefoil knot. *Science* **365**, 272–276 (2019).

22 Fan, Y.-Y. et al. An isolable catenane consisting of two Möbius conjugated nanohoops. *Nat. Commun.* 9, 3037 (2018).

23 Nishigaki, S. et al. Synthesis of belt- and Möbius-shaped cycloparaphenylenes by rhodium-catalyzed alkyne cyclotrimerization. *J. Am. Chem. Soc.* **141**, 14955–14960 (2019).

24 Wang, S. et al. Sulphur-embedded hydrocarbon belts: synthesis, structure and redox chemistry of cyclothianthrenes. *Angew. Chem., Int. Ed.* **60**, 18443–18447 (2021).

25 Segawa, Y. et al. Synthesis of a Möbius carbon nanobelt. *Nat. Synth.* **1**, 535–541 (2022).

26 Herges, R. Topology in chemistry: designing Möbius molecules. *Chem. Rev*. **106**, 4820–4842 (2006).

27 Jiang, X. et al. Kinetic control in the synthesis of a Möbius tris((ethynyl)[5] helicene) macrocycle using alkyne metathesis. *J. Am. Chem. Soc.* **142**, 6493–6498 (2020).

28 Schaller, G. R. et al. Design and synthesis of the first triply twisted Möbius annulene. *Nat. Chem.* **6**, 608–613 (2014).

29 Naulet, G. et al. Cyclic tris-[5]helicenes with single and triple twisted Möbius topologies and Möbius aromaticity. *Chem. Sci.* **9**, 8930–8936 (2018).

30 Murai, M., Hosokawa, N., Roy, D., Takai, K. Bismuth-catalyzed synthesis of polycyclic aromatic hydrocarbons (PAHs) with a phenanthrene backbone via cyclization and aromatization of 2-(2-arylphenyl)vinyl ethers. *Org. Lett.* **16**, 4134–4137 (2014).

31 Fan, W. et al. Facile synthesis of aryl-substituted cycloarenes via bismuth(iii)triflate-catalyzed cyclization ofvinyl ethers. *CCS Chem*. **2**, 1445–1452 (2020).

32 Fan, W., Han, Y., Wang, X., Hou, X & Wu, J. Expanded kekulenes. *J. Am. Chem. Soc.* **143**, 13908–13916 (2021).

33 Fan, W. et al. Synthesis and chiral resolution of twisted carbon nanobelts. *J. Am. Chem. Soc.* **143**, 15924–15929 (2021).

34 Khan, T. A., Fornefeld, T., Hübner, D., Vana, P. & Tietze, T. F. Palladium-catalyzed 4-fold domino reaction for the synthesis of a polymeric double switch. *Org. Lett.* **20**, 2007–2010 (2018).

35 Colwell, C. E., Price, T. W., Stauch, T. & Jasti, R. Strain visualization for strained macrocycles. *Chem. Sci.* **11**, 3923–3930 (2020).

36 Lu, T. & Chen, F. Multiwfn: A multifunctional wavefunction analyzer. *J. Comput. Chem.* **33**, 580–592 (2012).

37 Lu, T. & Chen, Q. A simple method of identifying π orbitals for non-planar systems and a protocol of studying π electronic structure. *Theor. Chem. Acc.* **139**, 25 (2020).

38 Pettersen, E. F. et al. UCSF Chimera—A visualization system for exploratory research and analysis. *J. Comput. Chem.* **25**, 1605–1612 (2004).

39 Hasegawa, M., Nojima, Y & Mazaki, Y. Circularly polarized luminescence in chiral π-conjugated macrocycles. *ChemPhotoChem* **5**, 1042–1058 (2021).

40 Satoa, S. et al. Chiral intertwined spirals and magnetic transition dipole moments dictated by cylinder helicity. *Proc. Natl. Acad. Sci. U. S. A*. **116**, 5194–5195 (2019).

Acknowledgements

J.W. acknowledges the financial support from A*STAR AME IRG grant (A20E5c0089) and NRF Investigatorship award (NRF-NRFI05-2019-0005). H.I. and T.M.F. thank the financial support from KAKENHI (20H05672 and 22K20527).

Author contributions

J.W. and W.F. conceived the concept, designed the project and prepared the manuscript. H.I. and T.M.F. performed the chiral HPLC experiments, CD measurements, data analysis and prepared the manuscript. W.F. performed the synthetic works. W.F., J.W., and X.H performed the photophysical measurements. S.W., Y.H., H.W. and Y.N. contributed to X-ray crystallographic analyses. W.F., Y.H., Q.Z., and Z.L. performed the computational studies.

Competing interests

The authors declare no competing interests.